Attosecond control of tunneling ionization and electron trajectories

New Journal of Physics
The open-access journal for physics

Attosecond control of tunneling ionization and electron trajectories

M Fieß[1,6,7], B Horvath[1,6,8], T Wittmann[1], W Helml[1,5], Y Cheng[2], B Zeng[2], Z Xu[2], A Scrinzi[3], J Gagnon[1], F Krausz[1,4] and R Kienberger[1,5]

[1] Max-Planck-Institute of Quantum Optics, Hans-Kopfermann-Straße 1, Garching, Germany
[2] State Key Laboratory of High Field Laser Physics, Shanghai Institute of Optics and Fine Mechanics, Chinese Academy of Sciences, PO Box 800-211, Shanghai 201800, China
[3] Ludwig-Maximilians-Universität München, Fakultät für Physik, Theresienstraße 37, 80333 München, Germany
[4] Ludwig-Maximilians-Universität München, Fakultät für Physik, Am Coulombwall 1, 85748 Garching, Germany
[5] Technische Universität München, Physik Department E11, James-Franck-Straße, 85748 Garching, Germany
[6] These authors contributed equally to this work.
E-mail: markus.fiess@mpq.mpg.de

New Journal of Physics **13** (2011) 033031 (10pp)
Received 12 January 2011
Published 21 March 2011
Online at http://www.njp.org/
doi:10.1088/1367-2630/13/3/033031

Abstract. We demonstrate the control of electron tunneling in the high-order harmonic generation process and subsequent positive-energy wavepacket propagation until recollision with the unprecedented precision of about 10 attoseconds. This is accomplished with waveforms synthesized from a few-cycle near-infrared pulse and its second harmonic. The presented attosecond control of few-cycle-driven high harmonics permits the generation of tunable isolated attosecond pulses, opening the prospects for a new class of attosecond pump–probe experiments.

[7] Author to whom any correspondence should be addressed.
[8] Present address: ABB Corporate Research Center, Segelhofstraße 1K, Baden-Daettwil, Switzerland.

Contents

1. Introduction

To date, isolated attosecond pulses are the shortest events at our disposal, offering direct, time-domain access to electron dynamics in atoms [1]–[4], molecules [5] and solids [6]. They emerge via high-order harmonic generation (HHG) from the exposure of atoms to sufficiently intense, linearly polarized optical radiation effectively confined to approximately a single wave period [7, 8], or from many-cycle pulses with modulated ellipticity [9]–[11]. Elementary steps in strong-field phenomena, such as HHG, above-threshold ionization and non-sequential ionization [12, 13], include tunneling ionization and the subsequent propagation of the emerging positive-energy electron wavepacket in the ionizing optical field. The synthesis of optical waveforms by superposition of the near-infrared (NIR) pulse and a second pulse with considerably longer or shorter carrier wavelength increased the flexibility in controlling strong-field processes [14]–[16]. So far, synthesized driver waveforms generated by the superposition of multi-cycle pulses of different carrier wavelengths have been used for the generation of high-harmonic continua [17]–[21]. However, the isolation of high-harmonic radiation that is generated only during one half-cycle of a multi-cycle driver waveform means that only a small fraction of the driver pulse energy is used for the HHG process. Therefore, we use linearly polarized carrier-envelope phase (CEP) stabilized waveforms synthesized from a few-cycle NIR pulse and its spectrally detuned second harmonic (SH) [22]. For the first time, this enabled us to demonstrate temporal control of tunneling ionization and electron trajectories in the high harmonic generation process on a 10 attosecond (asec) timescale. As a first application, we present the generation of tunable extreme ultraviolet (XUV) continua between 80 and 100 eV [23]. Since versatile attosecond spectroscopy calls for attosecond pulses with tailored photon energies adapted to the target under scrutiny, such a source of tunable isolated attosecond pulses will tremendously broaden the scope of attosecond pump–probe spectroscopy. It will enable a class of experiments where the photon energies should match the atomic resonances, such as in recent experiments that resolved a delay in the photoemission process [3, 6].

2. Experimental setup

We use few-cycle waveforms synthesized from a near-single-cycle wave carried at ~ 760 nm and a violet wave carried at ~ 430 nm produced by detuned SH generation from the

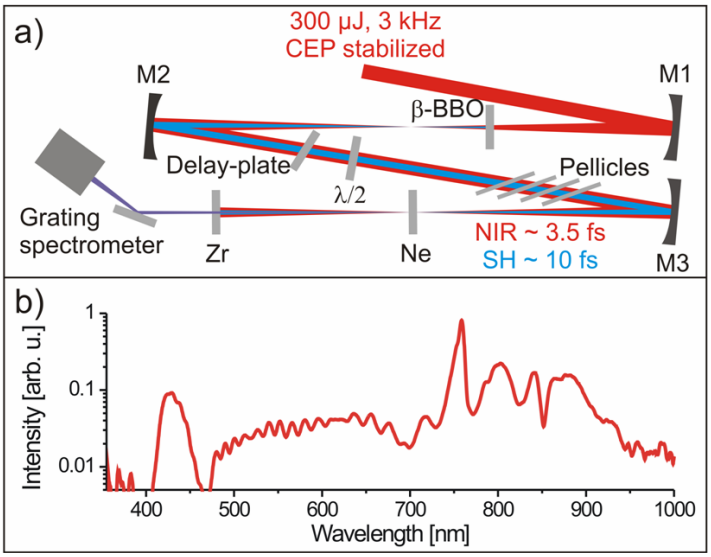

Figure 1. (a) Schematic diagram of the setup. Mirrors M1 and M2, with an identical radius of curvature (ROC) of − 750 mm, focus and recollimate the beam for SH generation in a 100 μm thick β-BBO crystal. A 150 μm thick delay plate (α-BBO) controls the synthesized waveform. A half-wave plate and pellicles set a linear polarization of the synthesized wave for HHG in a Ne target after focusing with M3 (ROC = −1000 mm). After filtering with a 1.0 μm thick Zr foil, high-harmonic spectra are recorded. (b) The synthesized spectrum of fundamental and SH fields.

NIR continuum. The experimental setup for waveform synthesis and HHG is shown in figure 1.

The experimental setup is based on a commercial laser system (Femtolaser Compact Pro, Femtolasers Produktions GmbH) adapted to the needs of the experiment, which generates NIR pulses with 300 μJ pulse energy, 760 nm carrier wavelength, 3 kHz repetition rate, stabilized CEP and negative chirp to compensate for the dispersion, which is later introduced by the subsequent optical components [24]. The fundamental NIR spectrum and the SH spectrum support a Fourier-limited pulse duration (full-width at half-maximum (FWHM)) of 3.5 and 10 fs, respectively. These laser pulses enter a vacuum system, at a pressure of 5×10^{-3} mbar, through an entrance window. The vacuum system contains the setup for waveform synthesis and HHG [25].

The NIR laser pulses are focused by a concave silver mirror, M1 (radius of curvature (ROC) of − 750 mm), and recollimated by a second concave silver mirror, M2 (ROC = −750 mm). In the converging beam between M1 and M2, a β-BBO crystal (100 μm thick, type I) is placed out of focus for SH generation at intensities just below its damage threshold. After recollimation, both the fundamental and the SH wave propagate through a retarding wave plate (α-BBO, 150 μm thick, $\theta = 57^\circ$; henceforth called the delay plate), which compensates for the positive group delay between the fundamental and the SH pulses introduced by the other optical components. The half-wave plate (crystal quartz, 42 μm thick, OptiSource LLC) turns the fundamental polarization by 90° and the SH polarization by 180° into one plane, which is optimal for high harmonic generation. Four pellicles at Brewster's angle serve for polarization

cleaning. The pulse in the NIR and the SH pulse in the violet with pulse energies of 180 and 11 μJ, respectively, are focused by a concave silver mirror, M3 (ROC $= -1000$ mm) in a gas target with a backing pressure of 200 mbar of neon. The substantial loss of pulse energy is attributed to Fresnel reflections on the uncoated β-BBO, delay plate, wave plate and pellicles. All mirrors were coated with silver due to its high reflectance in the spectral range of the NIR pulse at the expense of a reduced reflectance for the SH pulse. Due to the drastically decreasing reflectance of silver at wavelengths below 400 nm, the SH wavelength was set to 430 nm, conserving the highest possible SH pulse energy and leading to a detuned SH wave. The generated high harmonics were transmitted through a 1.0 μm thick Zr foil and spectrally resolved with a home-made grating spectrometer (Hitachi grating 001-0266, Roper Scientific XUV camera PIXIS XO). High-harmonic spectra have been recorded for different angles θ of the delay plate and different CEP settings of the fundamental pulse.

3. Alignment of the setup for waveform synthesis

HHG was first optimized with the NIR wave alone. Before entering the neon gas target, the NIR beam propagated through both the β-BBO and α-BBO crystals as well as through the wave plate and pellicles. The β-BBO crystal was placed 20 cm in front of the focus of the converging fundamental beam between mirrors M1 and M2 in figure 1, where the intensity of the fundamental pulse was too low for SH generation due to its large beam diameter. The positive chirp caused by the β-BBO, α-BBO, and the wave plate was compensated for by introducing negative chirp with a pair of wedges placed in the beam path of the laser system. This resulted in the shortest NIR pulse duration in the neon gas target and the highest XUV photon flux after HHG.

After optimizing HHG with the NIR pulse only, the distance between the β-BBO and the focus between mirrors M1 and M2 was decreased to 10 cm. Higher fundamental pulse intensities due to the smaller beam diameter resulted in typical SH generation conversion efficiencies of about 4%. HHG was optimized again with the synthesized $\omega + 2\omega$-waveform. The generated high-harmonic spectra show a strong dependence on both the CEP of the NIR pulse, which is set by means of the active CEP stabilization of the laser system, and the delay between the NIR and SH pulses, which is controlled by changing the θ-angle of the delay plate (α-BBO). Changing this θ-angle of the delay plate by 1.0° at normal incidence of the laser beam results in a calculated phase delay of 1.1 fs between the carrier waves of the fundamental and SH pulses. Since the CEP dephasing length is much longer than the path length variation during the θ-angle delay scan, the CEP of both pulses is nearly constant during the scan. Therefore, the change in the phase delay is approximately equal to the change in the group delay.

4. High-harmonic spectra

4.1. Delay scans

A series of high-harmonic spectra at different delays (delay scan) between the NIR pulse and the SH pulse is shown in figure 2(a). In this delay scan, the delay was changed, whereas the CEP was kept constant. The data reveal a periodicity of 1.4 fs in perfect agreement with the period of the SH wave at 430 nm. The high-harmonic spectra have been acquired in delay steps of 11 asec. XUV photons with energies below 70 eV are strongly suppressed by the zirconium filter and

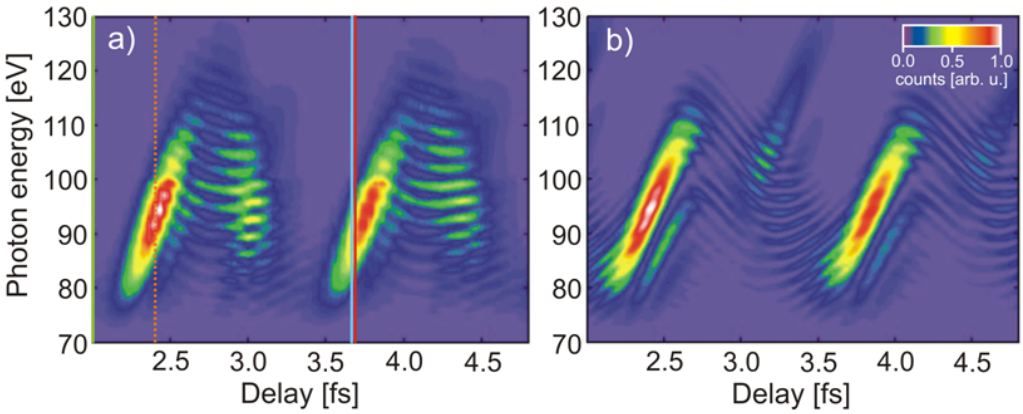

Figure 2. (a) Series of measured high-harmonic spectra at different delays between the NIR and SH waves. The solid blue and red vertical lines mark a delay range of 55 asec, demonstrating attosecond control of the electron trajectories in the HHG process in figure 5(b). The solid green and the dotted orange vertical lines mark the high-harmonic spectra shown in figure 5(a) with highest intensity contrast. (b) Calculated high-harmonic spectra based on the experimental parameters used.

the diffraction grating (see figures 1(a) and 4(b)). In the depicted energy range, the XUV flux of more than 5×10^9 photons s^{-1} has been measured taking into account the well-known filter transmission and the constant spectral response of the CCD detector.

Figure 3 shows that a change in the CEP leads to a transition from continuous to modulated high-harmonic spectra and vice versa. Changing the CEP by 2π led to identical delay scans. Replacing the zirconium filter with an aluminum filter and measuring delay scans below the aluminum absorption edge results in modulated XUV spectra [26]. Even harmonics can be observed at energies below the cutoff of the high-harmonic spectra. Increasing the SH pulse energy increases the maximum photon energy of the observable even high harmonics.

4.2. Tunable extreme ultraviolet (XUV) continua

Figure 2(a) shows two delay ranges with continuous XUV spectra and another two delay ranges with modulated XUV spectra. As demonstrated in figure 4(a), the carrier photon energy of the continuous XUV spectra can be shifted between 80 and 100 eV by varying the delay between the NIR and SH pulses in a range of 320 asec. The tunable XUV continua support a Fourier-limited pulse duration of less than 160 asec.

4.3. Attosecond control of high-harmonic spectra

Selected high-harmonic spectra of figure 2(a), which are separated by a delay of only 400 asec, are shown in figure 5(a), demonstrating attosecond control of the intensity of the emitted high-harmonic radiation, which is governed by the tunneling probability as the first step in the high harmonic generation process. Furthermore, figure 5(b) and repeated measurements reveal that changes in the delay between the NIR and SH waves as small as 11 asec give rise to significant, reproducible changes in the spectral distribution of the XUV continua. These

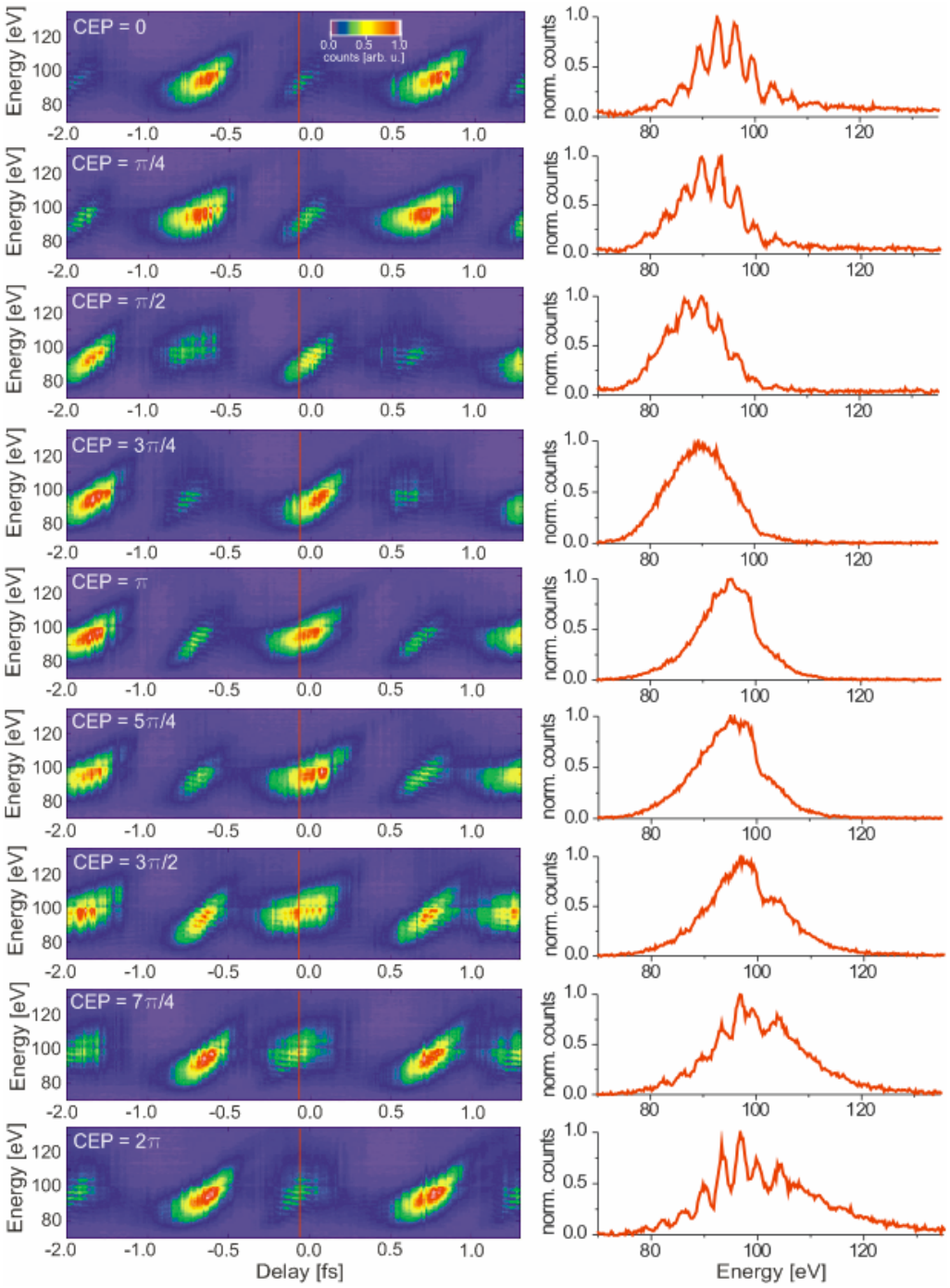

Figure 3. Delay scans for different CEP settings of the NIR wave. Altering the CEP leads to a change from continuous to modulated XUV spectra, which are marked by red vertical lines in the delay scans on the left side. CEP and delay are relative and not connected with the absolute values as defined in figure 2.

include a shift in the carrier photon energy of the emerging isolated attosecond pulses, which is determined by the ponderomotive energy the electron acquires during its propagation along trajectories between the tunneling and recombination events. Thus, shaping the driving optical

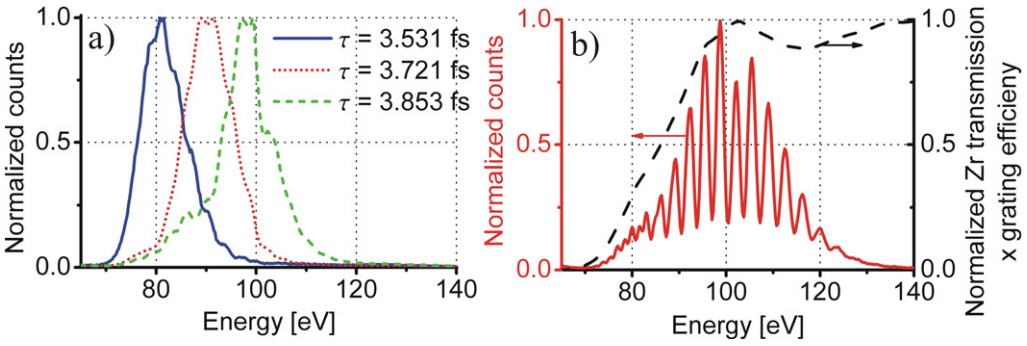

Figure 4. (a) Tunable high-harmonic spectra taken from figure 2(a). (b) Modulated high-harmonic spectrum taken from figure 2(a) at an absolute delay of $\tau = 4.244$ fs, which demonstrates a spectral resolution of the grating spectrometer of better than 0.8 eV. Delays are defined as in figure 2.

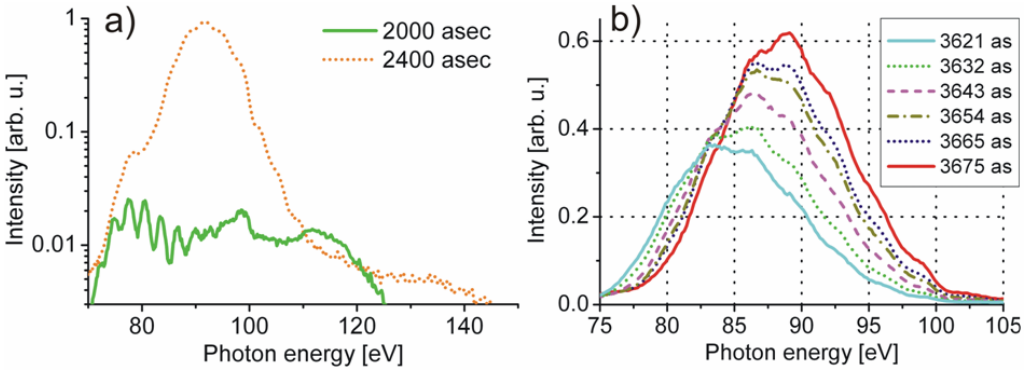

Figure 5. (a) Increase in the high-harmonic intensity by two orders of magnitude caused by a delay change of 400 asec. (b) Evolution of high-harmonic spectra in steps of 11 asec within a delay range of only 55 asec. Controlling the tunneling probability and the electron trajectory on an attosecond timescale allows for varying both the photon energy and the intensity of the emitted XUV continua. Delays are defined as in figure 2.

waveform on a timescale of merely a few attoseconds allows for unprecedented control of electron tunneling and electron trajectories in the HHG process.

5. Theory

Figure 2(b) shows simulations in our experimental conditions that unambiguously identify the driver waveform of each high-harmonic spectrum. These calculations confirmed that the short NIR pulse duration of only 3.5 fs is a condition for the observation of tunable XUV continua as presented in figure 2(a). An exact measurement of the NIR pulse duration is given by Fieß *et al* [27]. The simulated scan is obtained by using single-atom HHG calculations within the strong field approximation (SFA) [28]. Since the contributions of short trajectories are preferentially selected in this experiment by optimizing the focal conditions, the contributions of

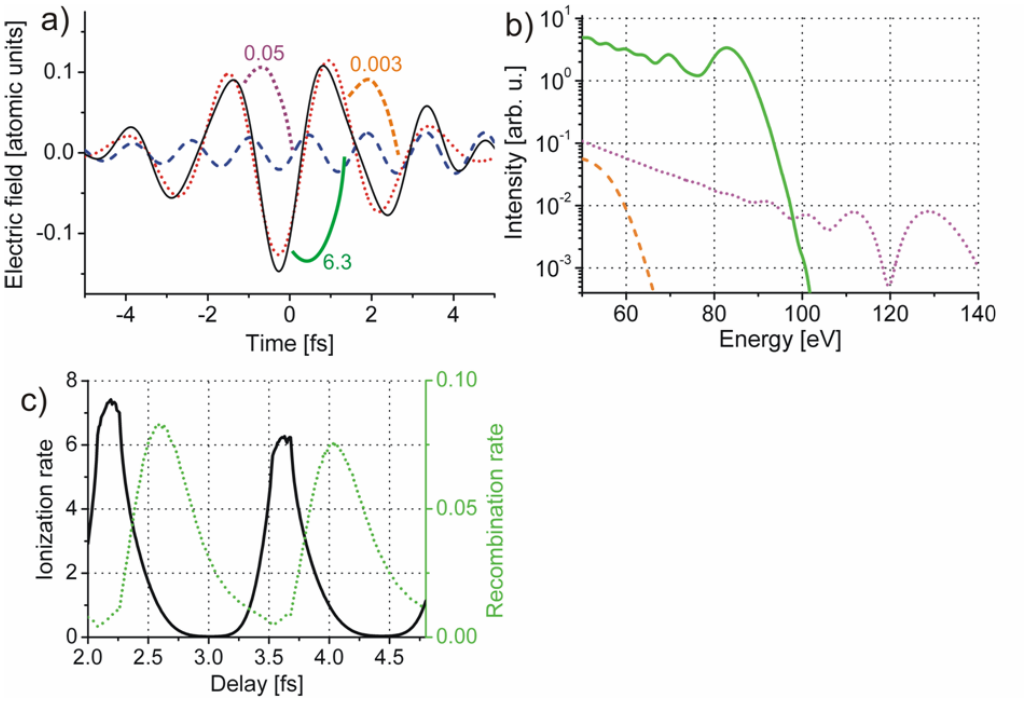

Figure 6. (a) Calculated waveform of the fundamental pulse (red dotted line), the SH pulse (blue dashed line) and their superposition (black solid line) at a delay of 3643 asec in figure 2(b). Classical electron trajectories of maximum return energy and their ionization rates in units of 10^{-4} per atomic time unit are also indicated. (b) Calculated high-harmonic spectra generated by the corresponding bundles of electron trajectories. (c) Evolution of the ionization rate (solid line) and recombination rate (dotted line) in units of 10^{-4} of trajectories resulting in an XUV photon energy of 85 eV generated within the half-cycle marked by the green solid line in (a) versus the delay between the NIR and SH pulses.

the long trajectories are removed from the SFA integration by including only the excursion times with $0 < \tau < 0.65T$, where T is the period of the fundamental wave at 760 nm wavelength [29]. The driving electric field is described as

$$E(t) = E_{\omega 1}\{\exp[-2\ln(2)\cdot t^2/\tau_1^2]\cos(\omega_1 t + \phi_1) + \sqrt{A}\cdot\exp[-2\ln(2)\cdot(t-t_0)^2/\tau_2^2]\cos[\omega_2(t-t_0)+2\phi_1]\}, \quad (1)$$

where E is the electric field amplitude of the fundamental wave and $\sqrt{A} = E_{\omega 2}/E_{\omega 1}$ is the ratio of the field amplitudes of the SH and fundamental waves. The τ_i, ω_i and ϕ_i are, respectively, the pulse durations (FWHM of electric field intensity), angular frequencies and CEPs of the fundamental wave ($i = 1$) and its SH ($i = 2$). In figures 2–4, absolute delays between the fundamental wave and its SH are defined by the parameter t_0. High-harmonic spectra are obtained by performing the Fourier transform of the acceleration of the dipole moment. In our simulation, the peak laser intensity of the fundamental pulse is $5.7 \times 10^{14}\,\mathrm{W\,cm^{-2}}$, and the ratio of the fundamental and SH field amplitudes is chosen to be $\sqrt{A} = 0.2$. The central wavelengths of the fundamental wave and its detuned SH are set at 760 and 430 nm, respectively. The pulse duration of the NIR and SH waves is set to 3.5 and 10 fs, respectively.

The best match between the experimental and theoretical results was achieved for a CEP of $\phi_1 = 220^\circ$.

Figure 6(a) shows the calculated NIR and SH waves as well as their superposition at a delay of 3643 asec. Ionization rates of three electron trajectories are also given. A further analysis in figure 6(b) reveals that only high harmonics that are generated during one half-cycle indicated by the green trajectory in figure 6(a) contribute to the intense XUV continuum, leading to the formation of an isolated attosecond pulse. Other half-cycles do not contribute to the energy range above 50 eV since either their ionization rate or their XUV photon energy is reduced by the contribution of the SH wave to the driving waveform. Figure 6(c) shows the calculated delay dependence of the ionization and recombination rates of electron trajectories within the half-cycle marked by the green solid line in figure 6(a), resulting in an XUV photon energy of 85 eV. The product of the depicted ionization and recombination rates reflects the changing high harmonic intensity at 85 eV in figure 2.

6. Summary

In conclusion, we have demonstrated attosecond control of electron tunneling and electron trajectories in the high harmonic generation process on a timescale of 10 asec. The calculations are in good agreement with the measured results and confirm the achieved control of electron trajectories in the HHG process. The capability of steering these two elementary processes with tailored optical waveforms holds promise for deeper insights into a broad range of strong-field processes and allows for their unprecedented temporal control. This work demonstrates the possibility of exploiting this control for generating continuously tunable single-attosecond pulses without the need for lossy optical elements. The enhanced degree of control at reduced losses is expected to significantly broaden the range of applications of attosecond pulses.

Acknowledgments

We thank A L Cavalieri for valuable experimental support. YC, BZ and ZX acknowledge funding from the National Basic Research Program of China (grant no. 2006CB80600). This work was supported by the Munich Center for Advanced Photonics. RK acknowledges funding from the Alexander von Humboldt Foundation (Sofja Kovalevskaja Award) and an ERC Starting Grant. MF is grateful to Studienstiftung des deutschen Volkes.

References

[1] Drescher M, Hentschel M, Kienberger R, Uiberacker M, Yakovlev V, Scrinzi A, Westerwalbesloh Th, Kleineberg U, Heinzmann U and Krausz F 2002 *Nature* **419** 803
[2] Uiberacker M *et al* 2007 *Nature* **446** 627
[3] Schultze M *et al* 2010 *Science* **328** 1658
[4] Goulielmakis E *et al* 2010 *Nature* **466** 739
[5] Sansone G *et al* 2010 *Nature* **465** 763
[6] Cavalieri A L *et al* 2007 *Nature* **449** 1029
[7] Christov I P, Murnane M M and Kapteyn H C 1997 *Phys. Rev. Lett.* **78** 1251
[8] Hentschel M, Kienberger R, Spielmann Ch, Reider G A, Milosevic N, Brabec T, Corkum P, Heinzmann U, Drescher M and Krausz F 2001 *Nature* **414** 509
[9] Sansone G *et al* 2006 *Science* **314** 443

[10] Tzallas P, Skantzakis E, Kalpouzos C, Benis E P, Tsakiris G D and Charalambidis D 2007 *Nat. Phys.* **3** 846
[11] Mashiko H, Gilbertson S, Li C, Khan S D, Shakya M M, Moon E and Chang Z 2008 *Phys. Rev. Lett.* **100** 103906
[12] Lewenstein M, Balcou Ph, Ivanov M Yu, L'Huillier A and Corkum P B 1994 *Phys. Rev.* A **49** 2117
[13] Krausz F and Ivanov M 2009 *Rev. Mod. Phys.* **81** 163
[14] Pfeifer T, Gallmann L, Abel M J, Nagel P M, Neumark D M and Leone S R 2006 *Phys. Rev. Lett.* **97** 163901
[15] Zeng Z, Cheng Y, Song X, Li R and Xu Z 2007 *Phys. Rev. Lett.* **98** 203901
[16] Chipperfield L E, Robinson J S, Tisch J W G and Marangos J P 2009 *Phys. Rev. Lett.* **102** 063003
[17] Feng X, Gilbertson S, Mashiko H, Wang H, Khan S D, Chini M, Wu Y, Zhao K and Chang Z 2009 *Phys. Rev. Lett.* **103** 183901
[18] Vozzi C, Calegari F, Frassetto F, Poletto L, Sansone G, Villoresi P, Nisoli M, De, Silvestri S and Stagira S 2009 *Phys. Rev.* A **79** 033842
[19] Calegari F, Vozzi C, Negro M, Sansone G, Frassetto F, Poletto L, Villoresi P, Nisoli M, De Silvestri and Stagira S 2009 *Opt. Lett.* **34** 3125
[20] Bandulet H-C, Comtois D, Bisson E, Fleischer A, Pépin H, Kieffer J-C, Corkum P B and Villeneuve D M 2010 *Phys. Rev.* A **81** 013803
[21] Takahashi E J, Lan P, Mücke O D, Nabekawa Y and Midorikawa K 2010 *Phys. Rev. Lett.* **104** 233901
[22] Merdji H, Auguste T, Boutu W, Caumes J-P, Carré B, Pfeifer T, Jullien A, Neumark D M and Leone S R 2007 *Opt. Lett.* **32** 3134
[23] Sansone G, Benedetti E, Vozzi C, Stagira S and Nisoli M 2010 *New J. Phys.* **10** 025006
[24] Cavalieri A L *et al* 2007 *New J. Phys.* **9** 242
[25] Oishi Y, Kaku M, Suda A, Kannari F and Midorikawa K 2006 *Opt. Express* **14** 7230
[26] Mansten E *et al* 2009 *Phys. Rev. Lett.* **102** 083002
[27] Fieß M, Schultze M, Goulielmakis E, Dennhardt B, Gagnon J, Hofstetter M, Kienberger R and Krausz F 2010 *Rev. Sci. Instrum.* **81** 093103
[28] Brabec T and Krausz F 2000 *Rev. Mod. Phys.* **72** 545–591
[29] Mansten E, Dahlström J M, Johnsson P, Swoboda M, L'Huillier A and Mauritsson J 2008 *New J. Phys.* **10** 083041